The Astronomical Journal, 148:98 (9pp), 2014 November doi:10.1088/0004-6256/148/5/98

A DETAILED STUDY OF THE STRUCTURE OF THE NESTED PLANETARY NEBULA, Hb 12, THE MATRYOSHKA NEBULA

D. M. Clark[1], J. A. López[1], M. L. Edwards[2], and C. Winge[3]
[1] Instituto de Astronomía, Universidad Nacional Autónoma de México, Campus Ensenada, Ensenada, Baja California, 22860; dmclark@astrosen.unam.mx, jal@astrosen.unam.mx
[2] LBT Observatory, University of Arizona, 933 North Cherry Avenue, Tucson, AZ 85721, USA; medwards@lbto.org
[3] Gemini Observatory, Southern Operations Center, c/o AURA Inc., Casilla 603, La Serena, Chile; cwinge@gemini.edu
Received 2014 February 27; accepted 2014 September 4; published 2014 October 17

ABSTRACT

We present near-IR, integral field spectroscopic observations of the planetary nebula (PN) Hb 12 using Near-infrared Integral Field Spectrograph (NIFS) on Gemini-North. Combining NIFS with the adaptive optics system Altair, we provide a detailed study of the core and inner structure of this PN. We focus the analysis in the prominent emission lines [Fe II] (1.6436 μm), He I (2.0585 μm), H_2 (2.1214 μm), and Br_γ (2.16553 μm). We find that the [Fe II] emission traces a tilted system of bipolar lobes, with the northern lobe being redshifted and the southern lobe blueshifted. The [Fe II] emission is very faint at the core and only present close to the systemic velocity. There is no H_2 emission in the core, whereas the core is prominent in the He I and Br_γ recombination lines. The H_2 emission is concentrated in equatorial arcs of emission surrounding the core and expanding at $\sim$30 km s^{-1}. These arcs are compared with *Hubble Space Telescope* images and shown to represent nested loops belonging to the inner sections of a much larger bipolar structure that replicates the inner one. The He I and Br_γ emission from the core clearly show a cylindrical central cavity that seems to represent the inner walls of an equatorial density enhancement or torus. The torus is 0.″2 wide ($\equiv$200 AU radius at a distance of 2000 pc) and expanding at $\leqslant$30 km s^{-1}. The eastern wall of the inner torus is consistently more intense than the western wall, which could indicate the presence of an off-center star, such as is observed in the similar hourglass PN, MyCn 18. A bipolar outflow is also detected in Br_γ emerging within 0.″1 from the core at $\sim\pm$40 km s^{-1}.

Key words: ISM: jets and outflows – planetary nebulae: general – planetary nebulae: individual (Hb 12)

Online-only material: color figures

1. INTRODUCTION

Hb 12 is a young planetary nebula (PN) with a very bright core and an hourglass nebula with a dense and tight waist. It is akin to the PN MyCn 18 (Bryce et al. 1997) and the symbiotic nebula He 2-104 (Corradi et al. 2001), both of which have high-speed, collimated outflows. The nebular main axis of Hb 12 is nearly north–south (PA $\sim -10^\circ$) and tilted $\sim 30^\circ \pm 5^\circ$ with respect to the plane of the sky. Miranda & Solf (1989) find from the [N II] optical emission lines that the central region expands at only 16 km s^{-1}. Collimated, high-velocity bipolar outflows are also detected from [N II] optical lines emerging from the bright core, reaching projected velocities of $\sim\pm$120 km s^{-1} at distances $\sim$75″ away from the nucleus (Vaytet et al. 2009). Previous ground-based, deconvolved, 2.12 μm images reveal an unresolved complex structure in the central region on scales $\leqslant$1.″0 and a rich, emission line environment in the nebula (Hora & Latter 1996). The inner regions are dominated by UV-excited, fluorescent, H_2 emission (Dinerstein et al. 1988) and shock-excited [Fe II] emission has been detected within 10″ of the core in the polar regions (Welch et al. 1999). *Hubble Space Telescope* (*HST*) NICMOS images reveal a series of nested equatorial arcs (Hora et al. 2000; Kwok & Hsia 2007) surrounding the core of the hourglass. Hsia et al. (2006) suggested that Hb 12 has a binary nucleus, but this has not been confirmed by others (DeMarco 2009).

There are very few hourglass PNe among the group of young bipolars with the characteristics of Hb 12 or MyCn 18, a possible indication that this particular class of objects represents a short transition stage toward full bipolar development. It is therefore of interest to study their structural components for a better understanding of the evolution of bipolar PNe. Theories pertaining to the origin of the hourglass structure include binary nuclei given the similarities between some symbiotic nebulae and hourglass-type PNe, e.g., Schwarz & Corradi (1992), Soker (2000), Blackman et al. (2001).

In the present work, we use the Near-infrared Integral Field Spectrometer (NIFS) combined with the high spatial resolution provided by the adaptive optics system Altair to study in detail the inner regions of Hb 12. Specifically, we use the emission lines [Fe II] (1.6436 μm), He I (2.0585 μm), H_2 (2.1214 μm), and Br_γ (2.1655 μm), which are bright and show the best detail of the core and inner structure. Using the power of a data cube, we extract frames at specific wavelengths to follow the changes in the emission structure across each line. In addition to the core, our observations include two additional pointings, one 5″ north and one 5″ south of the nucleus. These pointings include inner sections of the lobe structure of Hb 12. To complement our analysis, we compare our observations of sections of the lobes and the core with both optical and near-IR *HST* observations.

We organize this paper as follows. We describe the observations in Section 2, present our results and discussion in Section 3, and end with our conclusions in Section 4.

2. OBSERVATIONS

Observations of Hb 12 were carried out using the integral field spectrograph, NIFS (McGregor et al. 2003), on Gemini North with the adaptive optics module Altair during the night of 2010 September 25 as part of the observing program

GN-2010B-Q-43. NIFS is an image-slicing IFU with a field of view of 2.″99 × 2.″97. It consists of 29 slices with rectangular spaxels with dimensions of 0.″103 × 0.″043. We observed this PN using three pointings, one on the nucleus, one north of the nucleus, and one south of the nucleus. These were chosen to study the inner regions and neighboring outflow of this hourglass PN. For each field, we took spectra using both the *H* and *K* gratings with the *JH* and *HK* filters, respectively. This covers a spectral range of 1.49 μm–1.80 μm in *H* and 1.99 μm–2.40 μm in *K*, with a spectral resolution of $R = 5290$, which is equivalent to a mean velocity resolution of 60 km s^{-1}. After wavelength calibration, the linear dispersion is 2.14×10^{-4} μm per pixel for the *K* grating and 1.6×10^{-4} μm per pixel for the *H* grating, equivalent to 30 km s^{-1} per pixel. To measure the sky emission, we offset by 5″ to the north for each pointing in an ABA pattern. Since the nucleus is much brighter than the regions off the nucleus, different exposure times for each pointing and filter band were required, ranging from 20 to 150 s. By using a telluric standard star, we estimated an adaptive-optics-corrected FWHM image quality of 0.″11 in *JH* and 0.″12 in *HK*. The angular sampling in the final IFU data cube for each spectrum corresponds to 0.″1 × 0.″1. All observations were reduced using the IRAF scripts provided on the NIFS page of the Gemini Web site. Each spectra was first sky-subtracted, then divided by the flat field exposures, and trimmed to arrange each spectra frame into a stack of the spectra for each slice. A bad pixel mask was applied, the data were rectified, and a wavelength solution derived from the arc lamps was fit. In the final step, we converted the pseudo long-slit data into a data cube, with right ascension, declination, and wavelength axes.

3. RESULTS AND DISCUSSION

The distance to Hb 12 is highly uncertain. It ranges from 2.24 kpc (Cahn et al. 1992), 8.1 kpc (Zhang 1995), to the extreme value of 14.25 kpc (Stanghellini & Hayworth 2010). Hb 12 is a low excitation PN (Hyung & Aller 1996; Sahai & Trauger 1998; Rudy et al. 1993) with its inner regions dominated by UV-excited, fluorescent, H_2 emission (Dinerstein et al. 1988). Radiative fluorescence has been shown to dominate over shock excitation in the inner core regions of young PNe (Smith et al. 2003) and to be correlated to the evolutionary stage of the post-asymptotic-giant-branch star, as this becomes hot enough to produce UV photons (García-Hernandez et al. 2002). All these are elements that firmly indicate that Hb 12 is indeed a young PN that has only recently started to ionize its surrounding shell. The angular extent of the bipolar lobes, from tip to tip, measured from the *HST* images, is ≈10″, which, for a distance of 14.25 kpc, are ≡ 0.7 pc. Additionally, Vaytet et al. (2009) have detected outflowing knots of material from Hb 12 at 75″ away from the nucleus traveling at de-projected speeds of 285 km s^{-1}. Adopting again the distance of 14.25 kpc would yield a kinematic age for these knots of 1.7×10^4 yr. Both the size of the bipolar nebula and traveling time for the knots seem to be highly implausible for a young, developing PN. Conversely, considering a ≈ 2 kpc distance, the size of the bipolar nebula and the kinematic age for the knots become ∼0.1 pc and 2.5×10^3 yr; these dimensions are much more in line with those expected for a young, developing PN. For this reason, in this paper, we shall assume a distance to the nebula of ≈2 kpc.

3.1. Lobes

We begin our analysis of Hb 12 by discussing the lobe structure of this PN. Figure 1 shows two *HST* NICMOS images,

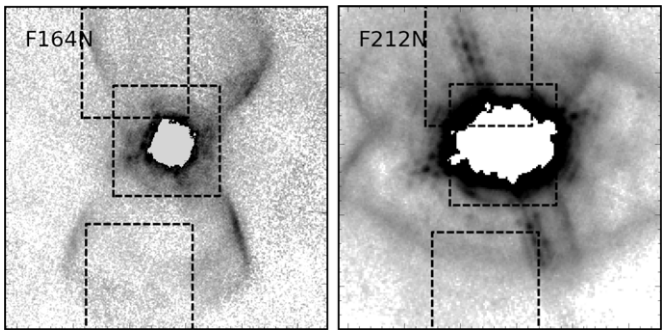

Figure 1. High-contrast, *HST* NICMOS images of Hb 12 showing the lobes and arcs associated with the PN. The central pixel values have been removed to allow for better contrast with the lobes without saturating the nucleus. All images are 9″ × 9″. Each frame includes 3″ × 3″ overlays of the three NIFS pointings for reference. *HST* archive images are from program 7365, PI: W. Latter.

filters F164N and F212N, from the Hubble Legacy Archive, where the NIFS pointings have been overlaid for reference.

Figure 2 displays a mosaic of NIFS images, where each row corresponds to a different emission line, namely, [Fe II] (1.6436 μm) and H_2 (2.1214 μm). Each row consists of six slices, each 9.″0 × 4.″2, of the data cube at various shifts in velocity from the line center, with a range in velocity shift from −60 km s^{-1} to 90 km s^{-1}. Each velocity channel is 30 km s^{-1} wide. In all cases the continuum has been subtracted and only the corresponding line emission is shown. All velocities have been corrected for heliocentric motion and are referred to a systemic velocity of 5 km s^{-1} (Vaytet et al. 2009).

The top row corresponds to the [Fe II] (1.6436 μm) line emission where the inner structures of the lobes can be clearly appreciated. The southern lobe is clearly detected from −30 km s^{-1} to 30 km s^{-1}, whereas the northern lobe is detected from 30 km s^{-1} to 90 km s^{-1}, indicating an inclination of the main nebular axis from the innermost region of the nebula with respect to the plane of the sky, with the northern lobe tilted away from the observer and the southern one toward the observer. This tilt of the main bipolar axis in the inner nebular region coincides with the results inferred by Hyung & Aller (1996) and Vaytet et al. (2009) from optical spectroscopy at larger scales. The [Fe II] lobes coincide spatially with the shock-excited [Fe II] "polar bubbles" described by (Welch et al. 1999). The bases of these lobes seem to emerge very close to the core, at ⩽1.″0, and outflow velocities reach ∼±90 ± 15 km s^{-1}. Their formation is most probably related to the collimated stellar wind interacting with the circumstellar material, producing the shocked [Fe II] emission that delineates the base of the bipolar lobes and was described by Welch et al. (1999) as "polar bubbles". The existence of these fast outflowing [Fe II] lobes was previously unknown. They also clearly indicate that the general inclination of the bipolar nebula at larger scales is shared by the innermost components.

The second row corresponds to the emission from molecular hydrogen, H_2 (2.1214 μm). There is practically no molecular hydrogen emission from the lobes; instead, what looks like a ring of emission is detected from −30 km s^{-1} to 60 km s^{-1}. This emission corresponds to the arcs described by Hora et al. (2000) and Kwok & Hsia (2007). The emission from these arcs is relatively bright in the central velocity channels corresponding to 0 km s^{-1} and 30 km s^{-1} and fainter in the contiguous outer channels at −30 km s^{-1} and 60 km s^{-1}. Only the northern or top part of the arcs is detected at −30 km s^{-1} (approaching), whereas only the southern or bottom part of the ring is detected at the velocity channel corresponding to 60 km s^{-1} (receding).

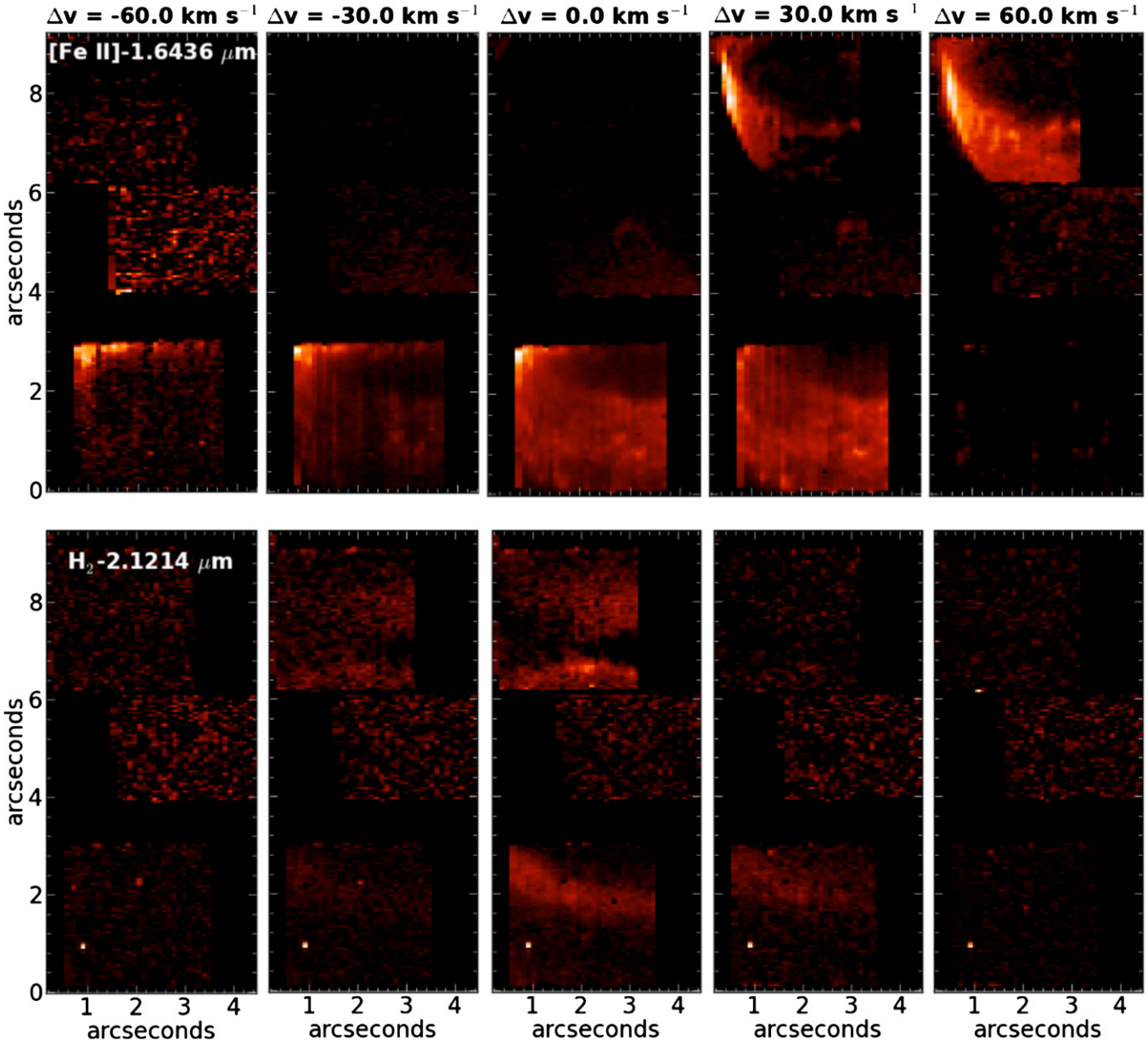

Figure 2. Mosaic of NIFS images; each row for a different emission line. Top row: [Fe II] (1.6436 μm). Bottom row: H_2 (2.1214 μm). Each row consists of six slices, each $9\farcs0 \times 4\farcs2$, covering a range in velocity shift from $-60\,\mathrm{km\,s^{-1}}$ to $90\,\mathrm{km\,s^{-1}}$, in steps of $30\,\mathrm{km\,s^{-1}}$. In all cases, the continuum has been subtracted. Velocities are referred to the heliocentric systemic velocity of $5\,\mathrm{km\,s^{-1}}$.

(A color version of this figure is available in the online journal.)

This indicates that the arcs are observed at a substantial tilt $\sim 45^\circ \pm 5^\circ$ and are expanding radially from the core at $\leqslant 45\,\mathrm{km\,s^{-1}}$. These arcs are also seen in the *HST* images from filters F110W, F160W, F175W, F212N, and F215N. Figure 3 is a mosaic of the *HST* NICMOS image F160W from the Hubble Legacy Archive showing different intensity levels where the system of nested loops of filaments are clearly displayed. The H_2 arcs detected with NIFS and shown in Figure 2 are indicated by arrows in the upper right panel in Figure 3, where it is apparent that a larger bipolar structure emerges from the deeper images and how this is connected with the equatorial arcs. Hora & Latter (1996) found evidence of this larger bipolar structure from H_2 ground-based observations, but its relation to the equatorial arcs was uncertain due to their limited spatial resolution. Hora et al. (2000) had suggested from the F160W and F212N NICMOS/*HST* images that Hb 12 could be a PN with multiple nested bipolar bubbles. The possible existence of this larger bipolar structure was speculated by Kwok & Hsia (2007) in relation to the equatorial arcs. The mosaic of images in Figure 3 and the NIFS data now confirm that the nested filaments or arcs correspond to an expanding and tilted equatorial structure that is part of this remarkably larger, outer, bipolar system that replicates the inner one, like a Russian Matryioshka doll. The highly structured equatorial filaments suggest their origin in a pulsed, mass-loss episode whose structure has been imprinted from its origin. The confirmation of this outer bipolar structure now firmly links Hb 12 to other few nebula with similar nested structures, such as Hen 2-104 and My Cn 18.

We detect only faint, diffuse emission from the He I (2.0585 μm) and Brγ (2.1656 μm) recombination lines in the lobes, close to the core, with no particular additional structure.

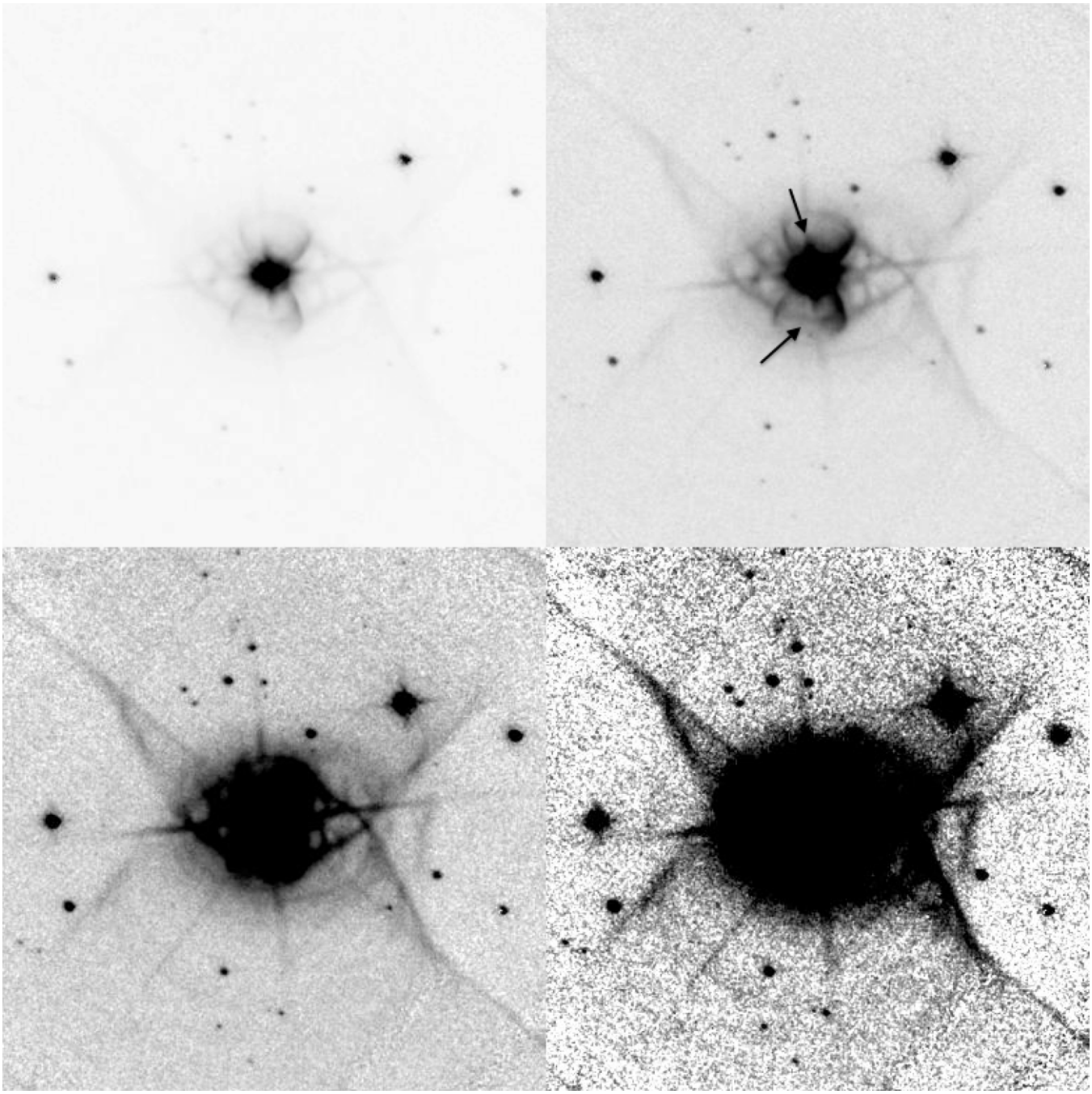

Figure 3. *HST* NICMOS F160W image from the HST Legacy Archive. It is shown at different intensity levels. The arrows in the top right panel point to the arcs detected in the NIFS H_2 frames shown in Figure 2. These images demonstrate that the system of equatorial arcs belong to an outer and larger bipolar structure. The field of view is $40'' \times 40''$.

3.2. Core

There is very little [Fe II] emission in the nucleus; only what seems like a small bubble ($\sim$0.″5 diameter) of faint emission is detected at the position of the core in the channel maps at 0 km s^{-1} and 30 km s^{-1} (see Figure 2). As mentioned above, there is neither H_2 emission in the core, nor in the lobes of Hb 12, which is consistent with the observations by Hora & Latter (1996).

The nucleus is bright in both the He I and Brγ recombination lines and the NIFS images show a considerable amount of detail here. As in Figure 2, Figure 4 presents images in these lines in velocity steps, but in this case showing only a $2'' \times 2''$ region around the nucleus. Images for each line are arranged horizontally, progressing in velocity steps from -90 km s^{-1} to 90 km s^{-1}. The nucleus is clearly seen split in both the He I (2.0585 μm) and Brγ lines, revealing a central cavity, most likely formed by an inner torus of approximate dimensions $0.''5 \times 0.''2$ and expanding at $\leqslant$15 km s^{-1}. This expansion velocity is derived from the long-slit spectral representation of the core, shown in Figure 6, considering that the bright nuclear emission is detected over the central two pixels, each 30 km s^{-1} wide, obtaining the expansion velocity as half the peak to peak velocity difference of the central line profile. All NIFS frames show the nucleus to be brighter on the eastern side than on the western side; this effect has also been noted in *HST* optical images

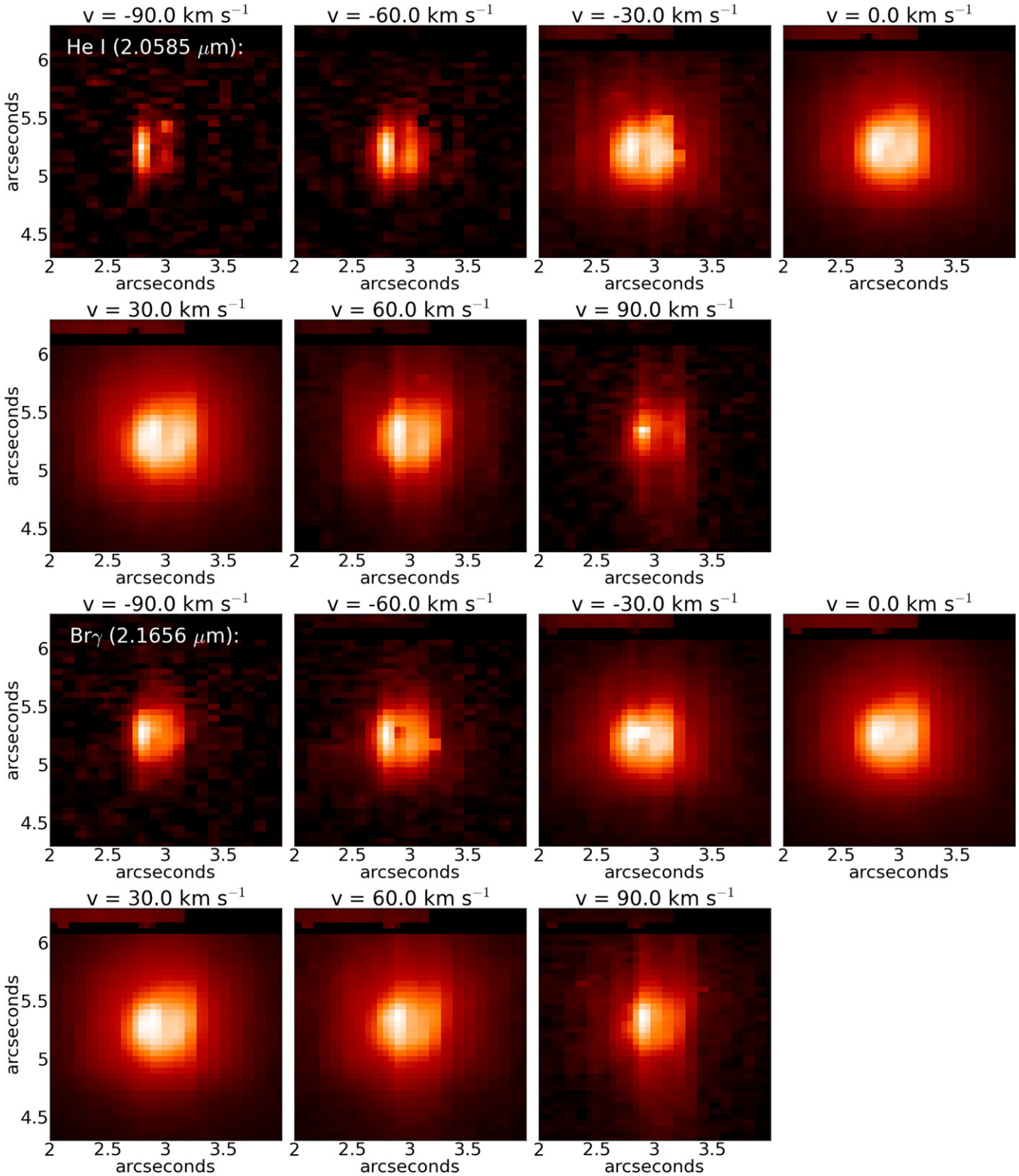

Figure 4. NIFS images of the nucleus of Hb 12, with offsets in velocity from line center for the two lines shown. Top and second rows: He I (2.0585 μm). Third and bottom rows: Brγ. All images are $2'' \times 2''$.

(A color version of this figure is available in the online journal.)

(Sahai & Trauger 1998; Balick 2003) and it shown here to extend to the near infrared.

Figure 5 presents horizontal cuts in intensity across the nucleus within a band of ± 4 pixels corresponding to each frame in Figure 4. The plots in Figure 5 show a definite displacement of the peak emissions arising from the walls of the toroid as a function of velocity. The peak emission from the eastern wall, which is brighter and better defined, shifts by $0\farcs1$ when the velocities turn positive. The western wall is fainter and less well defined. A vertical dashed line is shown in Figure 5 as reference

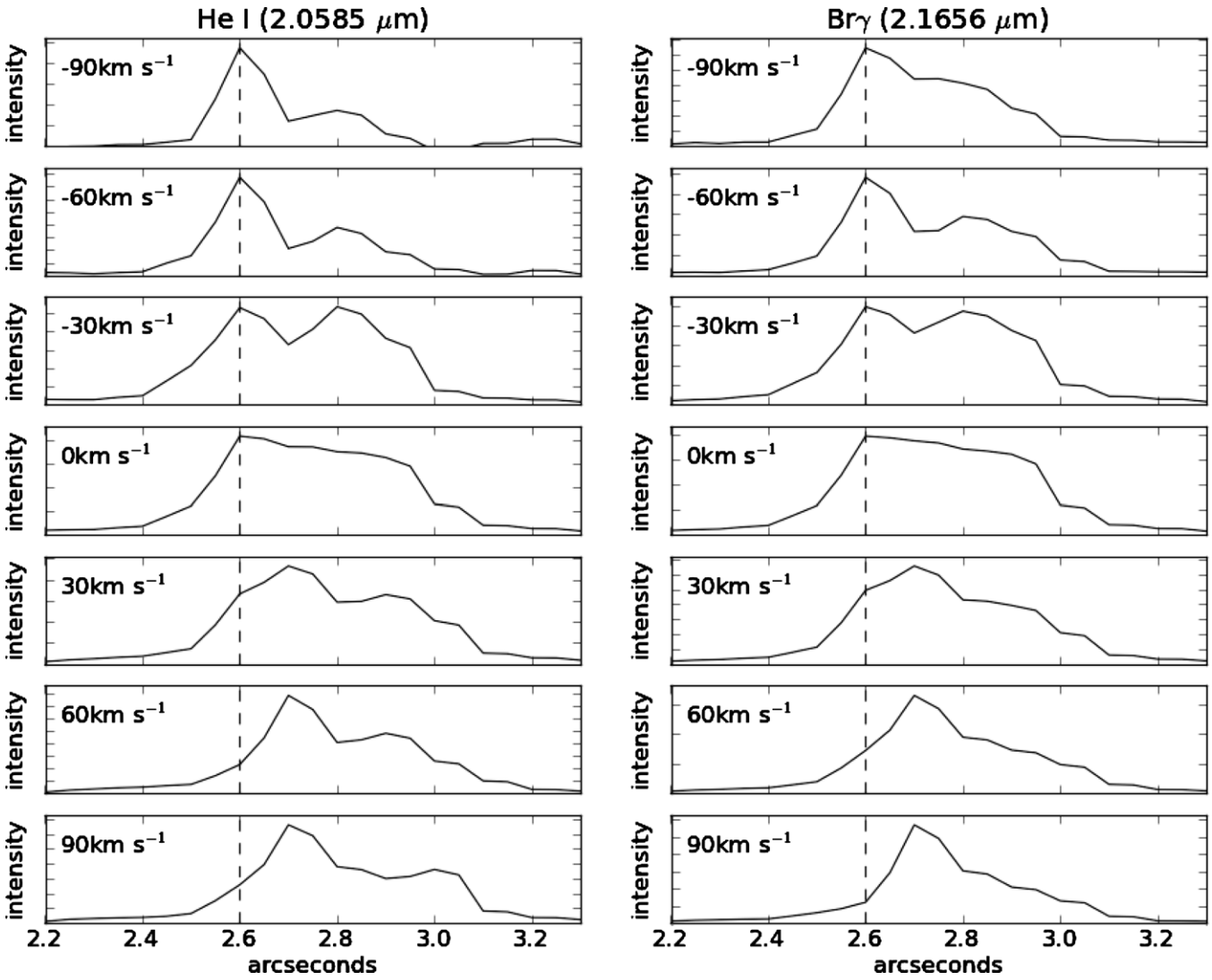

Figure 5. East–west plots across the nucleus for the panels in Figure 4. Each plot is the median from the central ±4 pixels. The walls of the inner torus produce the double-peak emission. The vertical dashed line is arbitrarily set as a reference to highlight the shift of the intensity profiles from negative to positive velocities.

to show the shift of the intensity profiles as the plots change sign in velocity. This effect can be understood in terms of a toroid or cylinder that has a slight rotation in position angle and whose upper section is tilted away from the observer and proves that the general tilt from the nebula derived at larger scales from optical spectroscopy is preserved at smaller scales, as is also revealed by the [Fe II] lobes emerging very close to the nucleus and down to the toroid at the very core. The tilt of a thick toroid with respect to the line of sight and the possibility that the as of yet undetected central star(s) may be located slightly off center, as in MyCn 18 (Sahai et al. 1999) would explain the uneven intensity distribution of the torus' walls and the shift in position with velocity of the intensity peaks. In addition, Figure 6 presents the Brγ line emission from the core as a pseudo long slit. The position–velocity (P–V) diagram reveals a bipolar structure in the line profile. Emission blobs are clearly present on both sides of the core emission at $\sim 45 \pm 15$ km s^{-1} and displaced by $\sim 0\farcs1$ ($\equiv$200 AU) from each other along the slit, with the redshifted blob slightly displaced to the north (up) from the core along the slit and the blueshifted blob to the south, as expected from the general inclination of the nebula. Fainter emission reaching ± 90 km s^{-1} can also be discerned in this long-slit image (compare with Figure 4). These blobs of emission are likely produced by mass-loaded wind mixed with ambient material emerging through the polar borders of the slowly expanding, dense torus which is tilted $25^\circ \pm 5^\circ$ with respect to the line of sight (see the next section). In this case, they represent the polar outflow that opens out to form the base of the lobes of the inner bipolar and show that the bipolar outflow originates very close to the core, within a projected distance of $\pm 0\farcs2$.

Assuming a distance of approximately 2 kpc to Hb 12, the average width or diameter of the torus, from the He I images, is $0\farcs2 \equiv 380$ AU and its average height is $0\farcs41 \equiv 800$ AU, i.e., it has a height to width ratio close to 2. Using several *HST* images, we measured the width of the lobes of the inner hourglass nebula at their widest section, obtaining an average width of 10,500 AU and an average length from to tip to tip of the lobes of 20,050 AU. Thus, the toroid is nearly 28 times narrower and 25 times shorter than the inner bipolar nebula. In order to provide a scale reference of the core structure described above, Figure 7 shows the F160W *HST* NICMOS image overlaid with an NIFS image of the core in the He I (2.0585 μm) line at a velocity shift of -30 km s^{-1} from the line center. The much

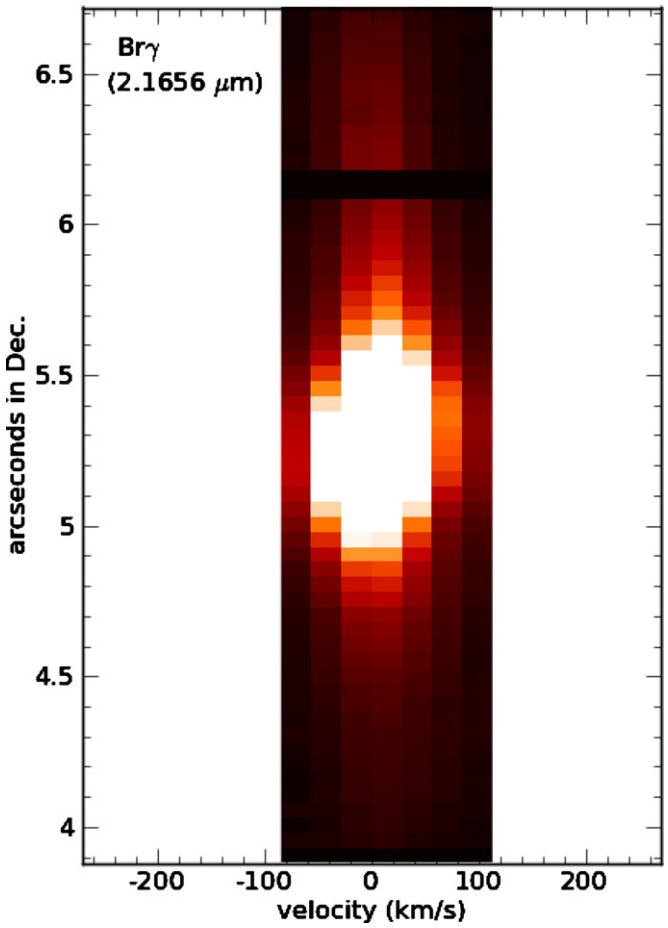

Figure 6. Brγ line emission from the nuclear region presented in a long-slit format. Blobs of emission on either side of the core, slightly displaced along the slit by 0.″1 from each other and at $\pm$45 km s^{-1} from the line center, are indicative of a bipolar flow emerging very close to the nucleus. Fainter emission reaches $\pm$90 km s^{-1}.

(A color version of this figure is available in the online journal.)

smaller size of the inner torus as compared to the width of the lobes of the hourglass nebula is apparent and provides insight into the collimation scales of the current bipolar outflow. If we were to assume a distance to Hb 12 of 14.25 kpc (Stanghellini & Hayworth 2010), this would imply a torus width of 0.015 pc, which is an unreasonable dimension for the collimating region where bipolarity originates in a developing young PN, as pointed out previously.

3.3. SHAPE Model of the Core

In order to explore the geometry of the core structure in more detail, we have built a SHAPE model (Steffen & López 2006; Steffen et al. 2011). This is a tool that can be used to obtain information on the three-dimensional (3D) structure of an extended object, such as a PN, by combining information from its kinematics and two-dimensional appearance on the sky. It requires spatially resolved spectra with a good coverage over the nebula and sufficient spectral resolution to determine the expansion pattern across the object. 3D structures are then built to represent the basic form of the nebula. These structures can be filled with particles or the particles can be distributed across the surface. Each system of particles can be given a unique velocity law. The program then produces synthetic spectra, or, in our case, synthetic channel maps, which can be compared

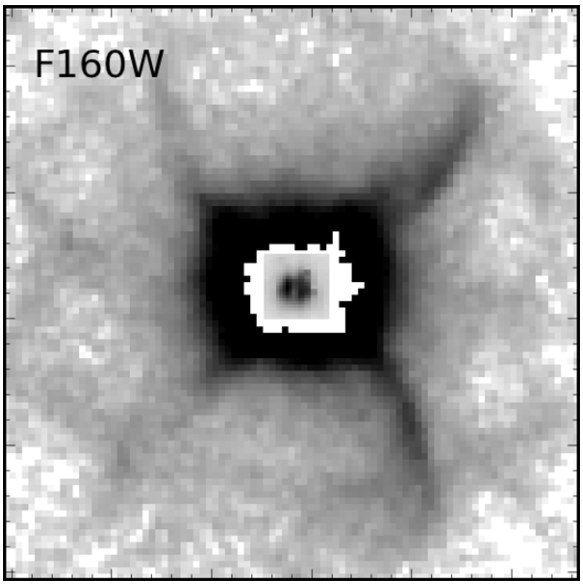

Figure 7. F160W *HST* image overlaid with a NIFS image of the core in the He I (2.0585 μm) line at a velocity shift of -30 km s^{-1}. The *HST* field of view is 9″ × 9″.

with the observations. An iterative process then leads to the best solution. The solution that best replicates the shape of the spectral elements in the individual velocity channels and their shift in position as the velocities go from redshifted to blueshifted is for a cylinder with an elliptical cross section, rotated by 10° in position angle and tilted by 25° $\pm$ 5° into the plane of the sky. The cylinder is enclosed within a thin sheet that provides the diffuse emission observed in the line profiles. Figure 8 shows the observed velocity channel maps from the core in the He I (2.0585 μm) emission line and below them the synthetic channel maps produced by the SHAPE model. The bottom panel of the figure shows the wireframe from two different perspectives and the final rendered image of the SHAPE model for the core region.

4. CONCLUSIONS

Using NIFS at Gemini North and the Altair adaptive optics system, we have obtained near diffraction limited data that have allowed us to make a detailed study of the structure of the young PN Hb 12. These data have shown that there is an inner system of [Fe II] bipolar lobes outflowing at projected velocities of $\pm$90 km s^{-1} and whose existence was previously unknown, though localized [Fe II]-emitting regions were previously detected north and south of the core (Welch et al. 1999). The [Fe II]-emitting bipolar lobes emerge very close to the core and most likely originate from shocked circumstellar material interacting with the stellar wind. This bipolar system shares the general tilt with respect to the plane of the sky derived from ground-based, optical observations of outer regions of the inner nebula, demonstrating that the general inclination of the bipolar nebula is shared by its innermost components. The NIFS data have been combined with archive *HST* images to reveal that the nested equatorial arcs previously detected in this nebula are indeed part of an outer and larger bipolar structure. These arcs are detected only in the NIFS H_2 images and are expanding at $\leqslant$45 km s^{-1}. At the core of the nebula, a tall toroid or cylinder of dimensions 0.″2 $\equiv$ 380 AU × 0.″41 $\equiv$ 800 AU (assuming a distance of 2 kpc) has been detected expanding at $\sim$15 km s^{-1}. The walls of this cylinder change in shape and position as a function

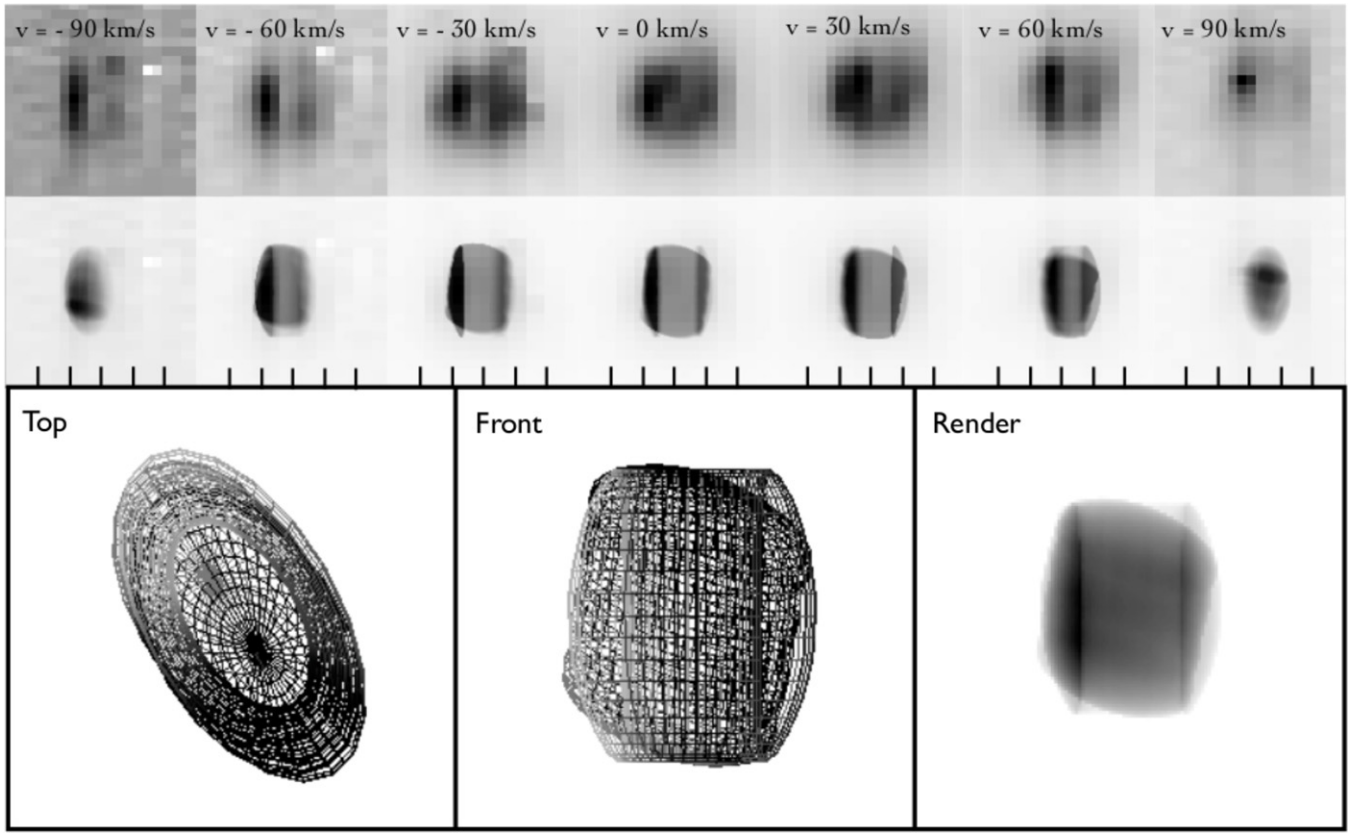

Figure 8. SHAPE 3D model of the core of Hb 12. The upper panel shows the observed velocity channel maps from the core in the He I (2.0585 μm) emission line and below them the synthetic maps produced by the SHAPE model. The bottom row shows the wireframe from two different perspectives and the final rendered image.

of velocity. We have constructed a SHAPE 3D model of the core region whose best solution yields a cylinder with an elliptical cross section rotated by 10° in position angle and tilted by 25° ± 5° into the plane of the sky, i.e., this cylindrical structure is also tilted in the same way as the bipolar lobes (i.e., the northern section away from the observer). A bipolar flow has also been detected in the Brγ emission line originating within 0.″1 from the core at ±45 km s^{-1} and reaching ±90 km s^{-1}within 0.″2 from the core, revealing a fast acceleration of the outflow in its early stages. The relative scale sizes and outflow speeds from this toroidal or cylindrical core structure in relation to the inner bipolar nebula provide important guidelines for hydrodynamical and collimation models. The general picture that emerges from these data for the formation of Hb 12 is that a pulsed, mass-loss episode produced the highly structured, nested, equatorial filaments, and, possibly, momentum-driven excess material formed the outer bipolar system. The equatorial filaments currently expand radially at $\leqslant$45 km s^{-1}. There is not yet any kinematic information on the expansion velocity of the outer, larger, bipolar lobes related to the nested equatorial filaments. The inner bipolar structure reaches projected velocities of ±90 km s^{-1}close to the core, within ±0.″2, indicating a steep initial acceleration rate. The core is formed by a tight and dense cylindrical region slowly expanding at only $\leqslant$15 km s^{-1}. It is unclear whether the high-speed knots found by Vaytet et al. (2009), up to 70 ″ away from the core and reaching ±120 km s^{-1}, were formed during the first mass-loss episode or during the creation of the second inner bipolar nebula at a later time. If these emission knots are indeed related to the second mass-loss episode, this indicates that the bipolar outflow accelerates at a steep rate within the first arcsec from the nucleus, during an energy-driven phase and then decline to a slower, momentum-driven rate, adopting a Hubble-type linear velocity law thereafter, as seen in many other PNe. A very similar scenario can apply to the symbiotic nebula Hen 2-104 (Santander-García et al. 2008) and the PN MyCn 18 (Bryce et al. 1997; Sahai et al. 1999). In these cases, an inner bipolar structure is replicated by an outer larger-scale bipolar nebula, and is reminiscent of a family of Matryoshka dolls. These type of nested structures are not common among planetary and symbiotic nebulae and suggests a common formation mechanism, most likely involving mass-loss processes influenced by a binary core. The central star of Hb 12 remains undetected; however, the uneven brightness in the walls of the core, where the eastern side of the nuclear structure is consistently brighter at most wavelengths, from optical to near infrared wavelengths, suggests the presence of an off-center star(s), as in the case of MyCn 18. In this case, it is likely that the star has remained hidden behind the eastern wall due to the tilt of the central cylinder with respect to the line of sight, as suggested by our SHAPE model.

Based on observations obtained at the Gemini Observatory, which is operated by the Association of Universities for Research in Astronomy, Inc., under a cooperative agreement with the NSF on behalf of the Gemini partnership: the National Science Foundation (United States), the National Research Council (Canada), CONICYT (Chile), the Australian Research Council (Australia), Ministério da Ciência, Tecnologia e Inovação (Brazil) and Ministerio de Ciencia, Tecnología e Innovación Productiva (Argentina). D. M. Clark and J. A. López gratefully acknowledge financial support from CONACYT (México) grant No. 178253.

REFERENCES

Balick, B. 2003, in ASP Conf Ser. 303, Symbiotic Stars Probing Stellar Evolution, ed. R. L. M. Corradi, R. Mikolajewska, & T. J. Mahoney (San Francisco, CA: ASP), 407
Blackman, E. G., Frank, A., & Welch, C. 2001, ApJ, 546, 288
Bryce, M., Lopez, J. A., Hollowat, A. J., & Meaburn, J. 1997, ApJ, 487, 161
Cahn, J. H., Kaler, J. B., & Stanghellini, L. 1992, A&AS, 94, 399
Corradi, R. L. M., Livio, M., Balick, B., Munari, U., & Schwarz, H. E. 2001, ApJ, 553, 211
DeMarco, O. 2009, PASP, 121, 316
Dinerstein, H. L., Lester, D. F., Carr, J. S., & Harvey, P. M. 1988, ApJL, 327, L27
García-Hernandez, D. A., Manchado, A., García-Lario, P., et al. 2002, A&A, 387, 955
Hora, J. L., & Latter, W. B. 1996, ApJ, 461, 288
Hora, J. L., Latter, W. B., Dayal, A., et al. 2000, in ASP Conf. Ser. 199, Asymmetrical Planetary Nebulae II: From Origins to Microstructures, ed. K. H. Kastner, N. Soker, & S. Rappaport (San Francisco, CA: ASP), 267
Hsia, C. H., Ip, W. H., & Li, J. Z. 2006, AJ, 131, 3040
Hyung, S., & Aller, L. H. 1996, MNRAS, 278, 551
Kwok, S., & Hsia, C. H. 2007, ApJ, 660, 341
McGregor, P. J., Hart, J., Conroy, P. G., et al. 2003, Proc. SPIE, 4841, 1581
Miranda, L. F., & Solf, J. 1989, A&A, 214, 353
Rudy, R. J., Rossano, G. S., & Erwin, P. 1993, AJ, 105, 1002
Sahai, R., Dayal, A., Watson, A. M., Trauger, J. T., et al. 1999, AJ, 118, 468
Sahai, R., & Trauger, J. T. 1998, AJ, 116, 1357
Santander-García, M., Corradi, R. L. M., Mampaso, A., et al. 2008, A&A, 485, 117
Schwarz, H. E., & Corradi, R. L. M. 1992, A&A, 96, 23
Smith, M. D., Stern, L., Kerr, T. H., & Chiar, J. E. 2003, MNRAS, 344, 262
Soker, N. 2000, ApJ, 538, 241
Stanghellini, L., & Hayworth, M. 2010, ApJ, 714, 1096
Steffen, W., Koning, N., Wenger, S., Morisset, C., & Magnor, M. 2011, IEEE Trans. Visualization Comp. Graphics, 17, 454
Steffen, W., & López, J. A. 2006, RMxAA, 42, 99
Vaytet, N. M. H., Rushton, A. P., Lloyd, M., et al. 2009, MNRAS, 398, 385
Welch, C. A., Frank, A., Pipher, J. L., Forrest, W. J., & Woodward, C. E. 1999, ApJL, 522, L69
Zhang, C. Y. 1995, ApJS, 98, 659